

RESEARCH

Automated quantification of myocardial tissue characteristics from native T_1 mapping using neural networks with Bayesian inference for uncertainty-based quality-control

Esther Puyol-Antón^{1*}, Bram Ruijsink^{1,2}, Christian F. Baumgartner³, Matthew Sinclair⁴, Ender Konukoglu³, Reza Razavi^{1,2} and Andrew P. King¹

*Correspondence:

esther.puyol.anton@kcl.ac.uk

¹School of Biomedical Engineering & Imaging Sciences, King's College London, Rayne Institute, 4th Floor Lambeth Wing St Thomas Hospital, Westminster Bridge Road, SE1 7EH London, UK

Full list of author information is available at the end of the article

Abstract

Background: Tissue characterisation with cardiovascular magnetic resonance (CMR) parametric mapping has the potential to detect and quantify both focal and diffuse alterations in myocardial structure not assessable by late gadolinium enhancement. Native T_1 mapping in particular has shown promise as a useful biomarker to support diagnostic, therapeutic and prognostic decision-making in ischaemic and non-ischaemic cardiomyopathies.

Methods: Convolutional neural networks (CNNs) with Bayesian inference are a category of artificial neural networks which model the uncertainty of the network output. This study presents an automated framework for tissue characterisation from native ShMOLLI T_1 mapping at 1.5 Tesla using a Probabilistic Hierarchical Segmentation (PHiSeg) network [1]. In addition, we use the uncertainty information provided by the PHiSeg network in a novel automated quality control (QC) step to identify uncertain T_1 values. The PHiSeg network and QC were validated against manual analysis on a cohort of the UK Biobank containing healthy subjects and chronic cardiomyopathy patients (N=100 for the PHiSeg network and N=700 for the QC). We used the proposed method to obtain reference T_1 ranges for the left ventricular myocardium in healthy subjects as well as common clinical cardiac conditions.

Results: T_1 values computed from automatic and manual segmentations were highly correlated ($r=0.97$). Bland-Altman analysis showed good agreement between the automated and manual measurements. The average Dice metric was 0.84 for the left ventricular myocardium. The sensitivity of detection of erroneous outputs was 91%. Finally, T_1 values were automatically derived from 14,683 CMR exams from the UK Biobank.

Conclusions: The proposed pipeline allows for automatic analysis of myocardial native T_1 mapping and includes a QC process to detect potentially erroneous results. T_1 reference values were presented for healthy subjects and common clinical cardiac conditions from the largest cohort to date using T_1 -mapping images.

Keywords: Native T_1 Mapping; Convolutional Neural Networks; Automatic Analysis; Cardiac MR Segmentation; Quality Control; UK Biobank

Background/Introduction

Cardiovascular magnetic resonance (CMR) provides insights into myocardial structure and function noninvasively, with high diagnostic accuracy and without ionising radiation. Late Gadolinium Enhancement (LGE) has become the reference standard for non-invasive imaging of myocardial scar and focal fibrosis in both ischaemic [2] and non-ischaemic cardiomyopathy [3]. LGE is useful in cardiac conditions which have stark regional differences within the myocardium, but it cannot correctly visualise myocardial pathology that is diffuse in nature and affects the myocardium uniformly. Examples include diffuse myocardial inflammation, fibrosis, hypertrophy, and infiltration [4]. In contrast, native T_1 -mapping provides quantitative myocardial tissue characterisation, without the need for gadolinium [5]. Previous work has shown that T_1 mapping can help to detect diffuse myocardial disease in early disease stages and aids in diagnosing the diseases' underlying cardiac dysfunction.

Despite its recognised potential, T_1 mapping analysis typically requires time-consuming manual segmentation of T_1 maps. Moreover, external factors, such as hematocrit and blood flow, impact the obtained values and create variability that reduces the ability to separate healthy from diseased myocardium. Several blood correction models have been proposed to limit the impact of external factors [6, 7, 8]. However, these methods have not been evaluated in large cohort studies. Automating T_1 analysis of myocardial tissue characterisation sequences could facilitate the clinical use of T_1 mapping and unlock the potential to obtain T_1 data in large populations.

In recent years, deep learning methods have shown great success in segmenting anatomical and pathological structures in medical images [9, 10, 11]. For many tasks, their accuracy is comparable to human-level performance, or even surpasses it. In the context of CMR imaging, semi-automatic and automatic techniques for cardiac cine [10, 9] and flow [12] imaging have been developed. One paper has proposed an automated segmentation method for native T_1 maps [11]. However, this method only extracted global left ventricle (LV) myocardial T_1 values, whereas regional assessment of septal and/or focal lesion T_1 values is typically used to characterise diseases [13, 14]. Furthermore, T_1 values were only reported for healthy subjects and a pooled group of cardiovascular diseases (CVD), without distinguishing between different myocardial disease processes and these values were not corrected for myocardial blood volume. In this paper we add further insight into the aforementioned areas.

Medical segmentation problems are often characterised by ambiguities, some of them inherent to the data such as poor contrast, inhomogeneous appearance and variations in imaging protocol, and some due to inter- and intra-observer variability in the annotated data used for training. To limit the effect of these factors and detect failed cases, some groups have proposed to incorporate quality control (QC) techniques [11, 10, 15]. We believe that modeling uncertainty at a per-pixel level is an important step in understanding the reliability of the segmentations and increasing clinicians' trust in the model's outputs. Several works have investigated

uncertainty estimation for deep neural networks [16, 17, 18]. A popular approach to account for the uncertainty in the learned model parameters is to use variational Bayesian methods, which are a family of techniques for approximating Bayesian inference over the network weights. These methods can be used to automatically segment the anatomy of interest, but additionally provide a pixel-wise uncertainty map of the confidence of the model in segmenting the input image. Budd *et al* [19] proposed to use this approach to automatically estimate fetal Head Circumference from Ultrasound imaging and provide real-time feedback on measurement robustness.

In this paper, we develop a tool for automated segmentation and analysis of T_1 maps. We use the PHiSeg network [1] to segment the images, and additionally use the generated uncertainty information in a novel QC process to identify uncertain (and potentially inaccurate) segmentations. To the best of our knowledge this is the first time that segmentation uncertainty information has been used for QC in medical image segmentation. By incorporating this QC process, our framework automatically controls the quality of the segmentations and rejects those that are uncertain. We hypothesise that this method can be used to derive high quality T_1 data without human interaction from large-scale databases. Using the proposed method we compute mean global and regional native T_1 values from 14,683 subjects from the UK Biobank, which represents the largest cohort for T_1 mapping images to date. We report reference values for healthy subjects and interrogate typical values obtained in important relevant subgroups of cardiomyopathies. In addition, we investigate if a blood correction model for T_1 [6] provides better discrimination between healthy and diseased myocardium.

Materials and Methods

UK Biobank dataset

CMR imaging was carried out on a 1.5 Tesla scanner (Siemens Healthcare, Erlangen, Germany). For each subject, the Shortened Modified Look-Locker Inversion recovery technique (ShMOLLI, WIP780B) was used to perform native (non-contrast) myocardial T_1 mapping in a single mid-ventricular short axis (SAX) slice (TE/TR/flip-angle (FA): 1.04ms/ 2.6ms/ 35°, voxel size 0.9 x 0.9 x 8.0 mm). The matrix size of all images was unified to 192 x 192. Details of the full image acquisition protocol can be found in [20].

As pre-processing, all of the CMR DICOM images were converted into NIfTI format. Training and validation data were obtained through manual segmentation of the images by an experienced CMR cardiologist. The LV endocardial and epicardial borders and the right ventricle (RV) endocardial border were traced using the ITK-SNAP interactive image visualisation and segmentation tool [21].

From the UK Biobank database, we first excluded any subject with systemic disease. Subsequently, we identified patients with CVD from the included cohort using ICD10 codes. We included 11 relevant groups of CVD: acute myocarditis,

aortic stenosis (AS), atrial fibrillation (AF), cardiac sarcoidosis, chronic coronary artery disease (CAD), dilated cardiomyopathy (DCM), hypertrophic cardiomyopathy (HCM), pheochromocytoma, obesity or takotsubo cardiomyopathy. Of the remaining subjects, those who had no history of CVD nor any cardiovascular risk factors were included as healthy subjects.

From the selected study population, we randomly chose three sub-cohorts: a set of 800 subjects (consisting of both healthy subjects as well as subjects with a wide variety of CVDs) for training, a set of 100 subjects (50 healthy subjects and 50 chronic cardiomyopathy subjects) for validation of the segmentations provided by the PHiSeg network, and a set of 700 subjects (500 healthy subjects and 200 chronic cardiomyopathy subjects) for the validation of the QC process.

Automated image analysis

The proposed workflow for automated T_1 map analysis is summarised in Figure 1 and described in detail in the following subsections.

Deep neural network with Bayesian inference for segmentation

In this work, we used a Probabilistic Hierarchical Segmentation (PHiSeg) network [1], a recently proposed deep learning network with Bayesian inference for segmentation of the LV blood pool, LV myocardium and RV blood pool from T_1 mapping images (Figure 1). The PHiSeg network employs convolutions to learn task-specific representations of the input data and predicts a pixel-wise segmentation from an input image based on this representation. In addition, an uncertainty map is generated which quantifies the pixel-wise uncertainty of the segmentation.

The PHiSeg network [1] models the segmentation problem at multiple scales from fine to coarse. Performing inference with this model using a conditional variational autoencoder approach results in a network architecture resembling the commonly used U-Net. However, in contrast to a U-Net, this network allows modelling of the joint probability of all pixels in the segmentation map. Specifically, it allows sampling multiple plausible segmentation hypotheses for an input image. In this manner, in addition to producing a per pixel prediction of the label class, it also allows estimation of the uncertainty corresponding to each pixel. The network architecture features a number of convolutional layers, each using a 3x3 kernel and a rectified linear unit (ReLU) activation function. After every three convolutions, the feature map is downsampled by a factor of 2 to learn more global scale features. After performing probabilistic inference at each level, the learned features are up-sampled and fused to produce a predicted segmentation mask and a uncertainty map at the original image resolution. To train the model, we aim to find the neural network parameters which maximise the evidence lower bound (ELBO), which models the marginal likelihood of the observed data. The general idea is that a higher marginal likelihood for a given model indicates a better fit of the data by that model and hence a greater probability that the model in question was the one that generated the data [22]. A detailed description of the method, as well as the network architecture can be found in [1].

Network training and testing

For training of the network, all images were cropped using the manual segmentation to the same size of 192×192 and intensity normalised to the range of $[0,1]$. Data augmentation was performed on-the-fly using random translations, rotations, scalings and intensity transformations to each mini-batch of images before feeding them to the network. Each mini-batch consisted of 20 native T_1 images. To optimise the loss function we used the Adam optimiser, with the momentum set to 0.9 and the learning rate to 10^{-3} . The models were trained for 50,000 iterations on a NVIDIA GeForce GTX TITAN GPU and the model with highest average Dice score (on the validation set) over all classes was selected.

Generating uncertainty maps

During test time, we used the PHiSeg network to sample T different segmentation output samples for a single given input (we used $T=100$). From these multiple segmentations the final predicted segmentation was calculated as the average softmax probability over all of the segmentation samples, and the uncertainty map was generated by computing the cross entropy between the mean segmentation mask and the segmentation samples.

Quality control

Our QC process comprises two steps, both based upon different aspects of the uncertainty information provided by the PHiSeg network. To train these QC steps, we manually labelled the PHiSeg-obtained segmentations as correct or incorrect in a cohort of 800 subjects (consisting of both healthy subjects as well as subjects with a wide variety of CVDs).

First, we used the ELBO output [1, 22] of the trained PHiSeg network to reject uncertain segmentations. The ELBO quantifies how likely it is that the segmentation is correct. We used the manual labellings to determine a threshold and any ELBO value above this threshold resulted in the segmentation being rejected.

The second QC step is defined as an image classification problem, where each image/segmentation pair is classified as accurate or inaccurate. The outputs of the PHiSeg network (i.e. the segmentation and uncertainty map) were used as input to a deep learning image classifier. For the image classifier, we used a VGG-16 CNN network [23], which consists of a stack of convolutional layers followed by three fully-connected layers for classification. Each convolutional layer uses a 3×3 kernel and is followed by batch normalisation and ReLU. Details of the VGG-16 network can be found in [23].

Data are rejected if either of these two QC steps fails. The combination of these two steps ensures that T_1 images acquired on different planes or with inaccurate segmentations are identified and rejected for further analysis.

T_1 map analysis

Myocardial T_1 values were measured from the mid-ventricular SAX slice for the whole myocardium, as well as for the interventricular septum and free-wall segments separately. From the predicted segmentation, the RV-LV intersection points

were automatically detected from the LV/RV segmentation masks (RV1 and RV2 in Figure 1) using the hit-or-miss transform, which is a morphological operation that detects a given configuration (or pattern) in an image. In our case, we aimed to detect the intersection between background, LV myocardium and RV labels. These RV-LV intersections were used to divide the LV myocardium mask into a LV interventricular septum (LVIVS) mask and a LV free-wall (LVFW) mask.

Myocardial T_1 blood correlation

For myocardial T_1 blood correlation, we used the model proposed by Nickander *et al* [6], which used a linear correlation between myocardial T_1 and blood measurements as follows:

$$T_1^{\text{corrected}} = T_1^{\text{uncorrected}} + \alpha \cdot (R_{\text{mean}} - R_{\text{patient}}), \quad (1)$$

where $T_1^{\text{uncorrected}}$ is the native myocardial T_1 value, R_{mean} is the mean R_1 for the patient cohort, and α is calculated as the slope of the linear regression between myocardial T_1 and blood T_1 measurements.

The blood T_1 value was computed from RV and LV blood pool regions of interest (ROI) in the mid-ventricular SAX T_1 map. To generate the LV and RV ROIs we eroded the LV/RV blood pool segmentations to generate a mask that has 1/3 of the area of the original mask (see Figure 2). To ensure that no papillary muscles or trabeculae were included, we rejected any pixel whose T_1 value was less than 1.5 times the interquartile range below the first quartile of the blood pool values. The blood T_1 value was calculated as the mean of the LV and RV values calculated in this way, and then converted to the T_1 relaxation rate ($R_1=1/T_1$).

Reference values

In total, we analysed CMR scans of 14,683 subjects (62 ± 22 yrs., 48% males) included in the UK Biobank cohort using our method. First, we derived reference values in 5,685 healthy subjects, selected using stringent criteria to exclude any disease or risk factor that impacts the heart or vasculature (see details in our previous paper [10]). Next, we analysed data of patients known to have one of 11 different CVD's. We also obtained indexed LV end diastolic volume (iLVEDV), LV ejection fraction (LVEF) and indexed LV mass (iLVM) from cine CMR data, using the automated method described in [10]. Outliers were defined a priori as values 3 interquartile ranges below the first or above the third quartile and they were removed from the analysis.

Evaluation of the method

We evaluated the performance of the automated network as follows:

Deep neural network with Bayesian inference: To validate the PHiSeg network, a cohort of 50 healthy volunteers and 50 chronic cardiomyopathy patients was selected and manually segmented. These subjects were not used for training the

PHiSeg network. We used the Dice metric to measure the degree of overlap between the automated and manual segmentations. The Dice metric has values between 0 and 1, where 0 denotes no overlap and 1 denotes perfect agreement. Furthermore, Bland-Altman analysis and Pearson's correlation were used to compare the obtained global LV native myocardial T_1 values, and the T_1 values in the LVIVS and LVFW, between the automated and manual segmentations.

Quality control: To assess the accuracy of the QC process, we manually labelled the PHiSeg obtained segmentations as correct or incorrect in a cohort of 500 healthy volunteers and 200 chronic cardiomyopathy patients, which are independent from the training cohort. We computed sensitivity (% of manually labelled as incorrect image/segmentation pairs that were correctly detected), specificity (% of manually labelled as correct image/segmentation pairs that were correctly identified), and balanced accuracy (averaged percentages of correct answers for correct/incorrect classes individually).

Statistical analysis

Statistical analysis was performed using Statsmodels, a Python library for statistical and econometric analysis [24]. Normality of distributions was tested with the Kolmogorov-Smirnov test. Categorical data are expressed as percentages, and continuous variables as mean \pm standard deviation (SD) or median and interquartile range, as appropriate. A paired 2-tailed Student's *t*-test was used to assess paired data, and an unpaired 2-tailed Student's *t*-test was used to assess unpaired samples. Comparison of more than three normally distributed variables was performed using analysis of variance (ANOVA, with Bonferroni post-hoc correction). For the Bland-Altman analysis, paired *t*-tests versus zero values were used to verify the significance of the biases, and paired *t*-tests were used to analyse the mean absolute errors of all parameters between healthy subjects and patients. Linear regression was performed to estimate the slope used for correction of myocardial T_1 from blood T_1 . The relationships between corrected and uncorrected mean native myocardial T_1 were investigated by computing the SD of the mean native myocardial T_1 , and evaluated for difference with a F-test. To investigate whether blood correction improved the discrimination between healthy subjects and patients with CVD's, we calculated the z-scores of the patients in each CVD group with respect to our healthy population for the uncorrected and corrected T_1 maps and compared the average z-scores using a paired 2-tailed Student's *t*-test. Associations between native T_1 values, clinical demographics and LV function were explored by single and multivariate linear regressions. In all cases, $p < 0.05$ denotes statistical significance. To compute reference values, healthy subjects were used as the study controls and unpaired *t*-tests were used for comparison.

Results

Deep neural network with Bayesian inference

Table 1 reports the Dice scores between automated and manual segmentations evaluated on the cohort of 100 subjects. Overall, the Dice score between manual and automated segmentations was 0.84 for the LV myocardium.

The Bland-Altman plot showed strong agreement between the pipeline and manual analysis, see Figure 3. There was a small negative bias for all of the native T_1 values (-5.04 ms, 5.89 ms and -4.97 for global LV, LVIVS and LVFW respectively). Table 2 shows the automatically and manually calculated T_1 values within the three regions averaged over the test cohort. There was no significant difference in mean absolute error between chronic cardiomyopathy patients and healthy volunteers for any of the T_1 values extracted except for LVIVS T_1 values for chronic cardiomyopathy patients. The automatically reconstructed T_1 maps showed a strong correlation with the T_1 values based on manual segmentations ($r=0.97$) (see Supplementary Figure 3).

Figure 4 shows an example of a manual segmentation, the predicted segmentation and the uncertainty map for a healthy subject and for a chronic cardiomyopathy patient. Note that the manual and the automatic segmentations agree well.

Quality control

The balanced accuracy for the QC process was 97.08%, the sensitivity was 90.08% and the specificity was 96.44%.

Figure 5 shows examples of uncertainty maps for a cohort of subjects that have been rejected by the QC steps. Note that the QC is able to identify inaccurate data with a wide range of underlying causes such as incorrect planning (i.e. images (a), (b), (c) and (d) in Figure 5), motion artefacts (i.e. images (e) and (f) in Figure 5) or segmentation failure (images (g) and (h) in Figure 5).

Uncertainty quantification

To understand the impact of uncertainty in the predicted T_1 values, from the test cohort that contains 50 healthy volunteers and 50 chronic cardiomyopathy patients, we computed the distribution of the global LV T_1 values over the T predicted segmentations. Figure 7 shows a graphical representations of the variability of these estimates. The solid lines indicate the mean T_1 values from the test cohort and the shaded region represents one SD of uncertainty.

Myocardial T_1 blood correlation

The constants from the linear regression model between the myocardial T_1 and the blood measurements were used to correct native myocardial T_1 values according to Equation 1. The global R^2 was 0.28 (which is comparable to that found in [6]) and the mean squared error was 106.4. The linear regression had a slope of -0.35 and an intercept of 935.

The mean uncorrected myocardial T_1 in the healthy cohort was 946.44 ± 61.64 , and the mean corrected myocardial T_1 in the healthy cohort was 927.62 ± 46.41 , showing a statistically significant decrease of the SD ($p < 0.001$).

Reference values

From the 14,683 subjects, 156 subjects were rejected by our QC process due to inaccurate T_1 segmentations. Subject characteristics are summarised in Table 3. Compared to healthy subjects, all patients were in the same age range; patients with obesity had statistically higher body mass index (BMI) and body surface area (BSA); patients with DCM, AF and chronic CAD had significantly lower LVEF (all $p < 0.05$); patients with HCM, AS and chronic CAD had significantly higher iLVM (all $p < 0.05$). Native T_1 in three different regions (LV, LVIVS, LVFW) in CVD subjects and in healthy subjects are shown in Table 5. Gender did not affect myocardial T_1 values significantly (2-way ANOVA, $p = 0.01$), and thus only overall T_1 values are reported.

Native T_1 values in typical tissue classes in CVD subjects and in healthy subjects for uncorrected and corrected myocardial LVIVS T_1 values are shown in Figure 6. Table 5 shows global and regional native correlated T_1 values. Compared to healthy subjects, patients with DCM, HCM, Takotsubo cardiomyopathy, acute myocarditis and cardiac sarcoidosis had significantly higher native T_1 values.

Finally, Table 4 shows LVIVS native correlated T_1 values stratified by age by decade (45 to 54, 55 to 64, and 65 to 74 years), and reported as mean and reference ranges (95% prediction intervals). Note that, in the first age range, i.e. 45-55, there were not enough data to compute the confidence interval for the AS group.

Discussion

In this work, we have proposed a fully automated pipeline with a novel quality control step to automatically quantify myocardial tissue from native T_1 mapping, which allows extraction of reference values from large-scale databases. The method is fast and scalable, overcoming limitations associated with current clinical CMR image analysis workflows, which are manual, time-consuming and prone to subjective error. The method has potential to automate T_1 mapping analyses from CMR in clinical practice and research. Using the proposed pipeline we present reference ranges for global and regional myocardial native T_1 in healthy subjects from the UK Biobank dataset and show that blood correction improves discrimination between healthy subjects and patients with CVD.

Automatic analysis with quality control

We validated our segmentation network by comparing between automated and manual analysis in a cohort of healthy and diseased subjects. Results show a strong agreement for both segmentations (see Table 1) as well as estimated T_1 values (Figures 3 and 3). Residual biases in automated T_1 calculations might not necessarily correspond to T_1 estimation errors but might be related to the different methods used to compute T_1 between manual and automatic analysis. Residual biases are within the range of inter- and intraobserver variabilities previously reported [25]. Also, residual biases (ranging between -4.97ms and -5.04ms) are consistent between healthy and cardiac patients and are unlikely to have significant clinical impact. The Dice scores we obtained are comparable to previous works [11].

Quality control techniques are essential to be able to translate deep learning algorithms into a clinical setting. However, many works proposed for the analysis of CMR data have not taken this need into account making it impossible to deploy them for the processing of large-scale databases. In our framework, we employed a novel approach that used the uncertainty information produced by a CNN with Bayesian inference to identify incorrect segmentations, which can be rejected or flagged for revision by an expert cardiologist. We show that this QC process yields over 90% sensitivity of detecting errors, getting close to clinical standards. One way to further optimize QC in our network would be to incorporate anatomical information into the uncertainty estimation. At the moment, segmentation errors of both RV and LV are accounted for similarly, while the segmentation of the LV is most important for T_1 calculations.

Reference values:

We used our framework to analyse native T_1 maps in an unprecedentedly large cohort of healthy volunteers and patients with heart disease. Using this cohort we were able to provide reference values for normal myocardium in aging subjects. T_1 values differ between different scanners, vendors and protocols. Our values can therefore not directly compare to other publications, but they are in agreement with results obtained in smaller cohorts of manual assessment [8, 26, 27]. We further used our cohort to interrogate T_1 values in patients with 11 different CVDs. We show that for CVDs in which diffuse myocardial disease is prominent (acute myocarditis, cardiac sarcoidosis, HCM, DCM and tako Tsubo disease) we detect significantly larger T_1 values. For the other CVD's, we show that T_1 values did not significantly change from healthy data. It is likely that the extent of myocardial damage in these groups is less high, explaining the lower T_1 values. There is large variability seen in native T_1 values, which is known to be caused by several factors, including intracardiac blood flow and hematocrite levels. We investigated a previously proposed method for correction of T_1 values based on blood pool T_1 dynamics [6]. This method has the benefit on working using image data alone, but has not previously been tested in a large cohort of patients. We demonstrate that indeed, discrimination between health and disease improves using blood pool correction. Whether this technique is better than using hematocrite-correction or other methods needs to be investigated in further studies. Investigating myocardial disease processes should include additional measures to native T_1 , such as extracellular volume or T_2 imaging. However, the data presented in our study remain valuable. The UK Biobank cohort will contain highly detailed imaging and non-imaging data and follow-up in nearly half a million subjects. On this large scale, new relationships between T_1 and population characteristics can yield important insights into development and progression of CVDs.

Limitations and future directions:

A limitation of our work is that the PHiSeg network was trained on a single dataset, the UK Biobank dataset, which is relatively homogeneous. To obtain similar performance in other databases it would be necessary to retrain the networks using a small amount of data. However, the proposed segmentation model and QC steps

will remain applicable.

Another limitation of this study is the lack of availability of paired LGE and native T_1 -mapping data to assess the correlation between these two measurements, and in which cases T_1 -mapping could provide a better insight into cardiac pathologies. Based on previous studies, it is known that T_1 -mapping may enable detection of early pathological processes, and serve as a tool for early diagnosis or screening, or differentiation of cardiomyopathies from normal phenotypes. The provided reference ranges could help to identify subjects at risk at an early stage.

The T_1 values presented in this study were derived using a single T_1 -mapping technique. It is important to take into account that even within the same T_1 -mapping technique, different versions of sequences can lead to small differences in T_1 -estimations. Therefore, it might not be possible to directly translate the T_1 values derived in this study to other T_1 -mapping techniques. In future work we aim to extend the automatic pipeline to be able to accurately segment T_1 -mapping data from different sequences/vendors, to make the proposed framework generalisable.

Conclusions

We presented and validated a pipeline for automated quantification of myocardial tissue from native T_1 -mapping. The proposed method uses the uncertainty of a deep learning segmentation network in a novel QC process to detect inaccurate segmentations. We used the proposed framework to obtain reference values from the largest cohort of subjects to date, which include data from healthy subjects and from patients with the most common myocardial tissue conditions.

List of abbreviations

AF	Atrial fibrillation
ANOVA	Analysis of variance
AS	Aortic stenosis
BMI	Body mass index
BPM	Beats per minute
BSA	Body surface area
CAD	Coronary artery disease
CMR	Cardiac magnetic resonance
CNN	Convolutional neural networks
CVAE	Conditional variational autoencoder
CVD	Cardiovascular disease
DCM	Dilated cardiomyopathy
ELBO	Evidence lower bound
HCM	Hypertrophic cardiomyopathy
iLVEDV	Indexed LV end diastolic volume
iLVM	LV mass index
LGE	Late gadolinium enhancement

LV	Left ventricle
LVEF	LV ejection fraction
LVIVS	Left ventricle interventricular septum
LFW	Left ventricle free-wall
QC	Quality control
PHiSeg	Probabilistic Hierarchical Segmentation
ReLU	Rectified linear unit
ROI	Regions of interest
RV	Right ventricle
SAX	Short axis
SD	Standard deviation

Ethics declarations

Ethics approval and consent to participate

UK Biobank has approval from the North West Research Ethics Committee (REC reference: 11/NW/0382).

Consent for publication

Not applicable.

Competing interests

MS is an employee of HeartFlow, Redwood City, California. All other authors have reported that they have no relationships relevant to the contents of this paper to disclose.

Acknowledgements

This research has been conducted mainly using the UK Biobank Resource under Application Number 17806. The authors wish to thank all UK Biobank participants and staff. This research has been conducted using a GPU generously donated by NVIDIA Corporation.

Funding

This work was supported by the Wellcome EPSRC Centre for Medical Engineering at Kings College London (WT 203148/Z/16/Z), the EPSRC (EP/R005516/1 and EP/P001009/1) and by the NIHR Cardiovascular MedTech Co-operative. The views expressed are those of the author(s) and not necessarily those of the NHS, the NIHR, EPSRC, or the Department of Health.

Availability of data and materials

The imaging data and manual annotations were provided by the UK Biobank Resource under Application Number 17806. Researchers can apply to use the UK Biobank data resource for health-related research in the public interest [28].

Author's contributions

Author contribution are as following: conception and study design (EPA, BR, RR and APK); development of algorithms and analysis software (EPA, CFB, EK and MS); data pre-processing (EPA and MS); data analysis (EPA and BR); clinical advice (BR and RR); manual image annotation (BR); interpretation of data and results (EPA, BR, RR and APK); drafting (EPA, BR and APK); revising (EPA, BR, CFB, EK, MS, RR and APK). All authors read and approved the final manuscript.

Author details

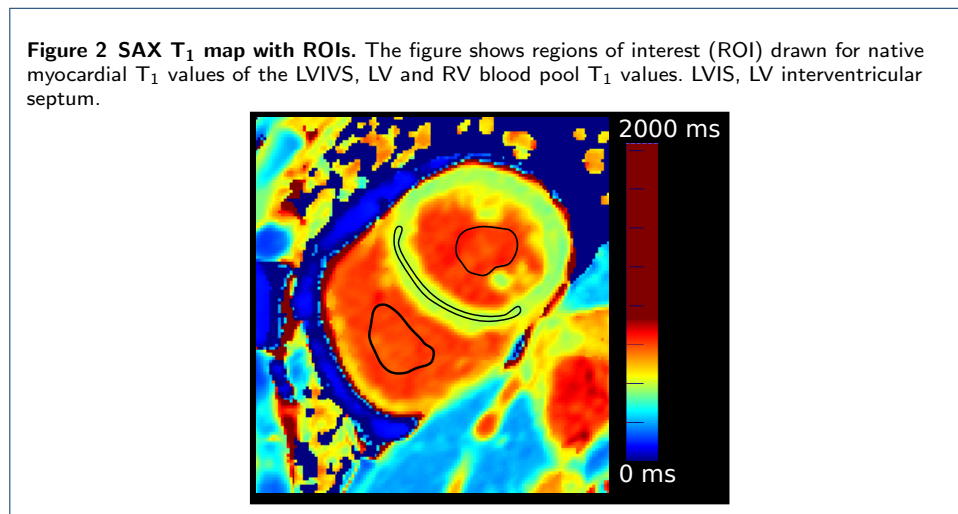
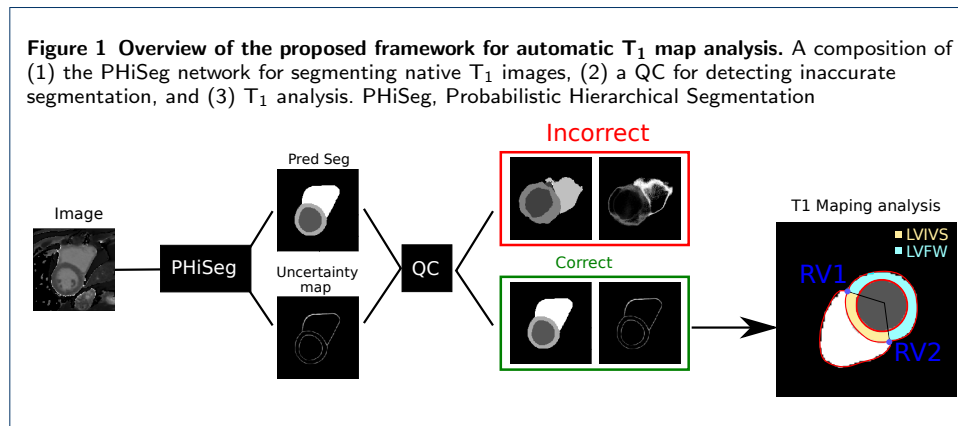
¹School of Biomedical Engineering & Imaging Sciences, King's College London, Rayne Institute, 4th Floor Lambeth Wing St Thomas Hospital, Westminster Bridge Road, SE1 7EH London, UK. ²Department of Adult and Paediatric Cardiology, Guy's and St Thomas' NHS Foundation Trust, London, UK. ³Computer Vision Lab, ETH Zürich, Sternwartstrasse 7, Zürich London, Switzerland. ⁴Biomedical Image Analysis Group, Department of Computing, Imperial College London, 3rd floor Huxley Building, 180 Queen's Gate, SW7 2AZ London, UK.

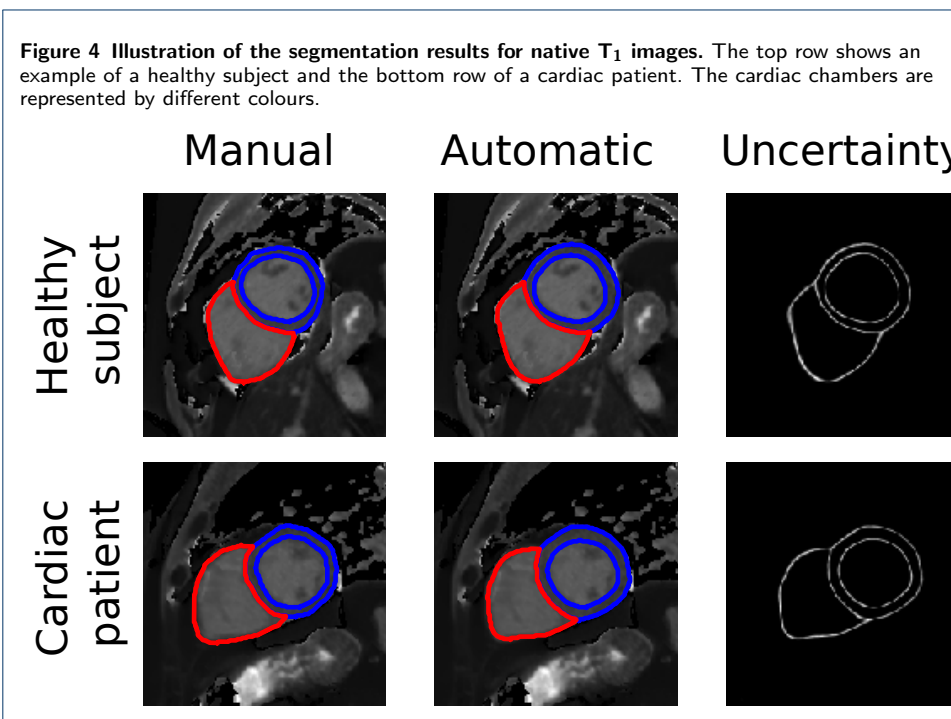
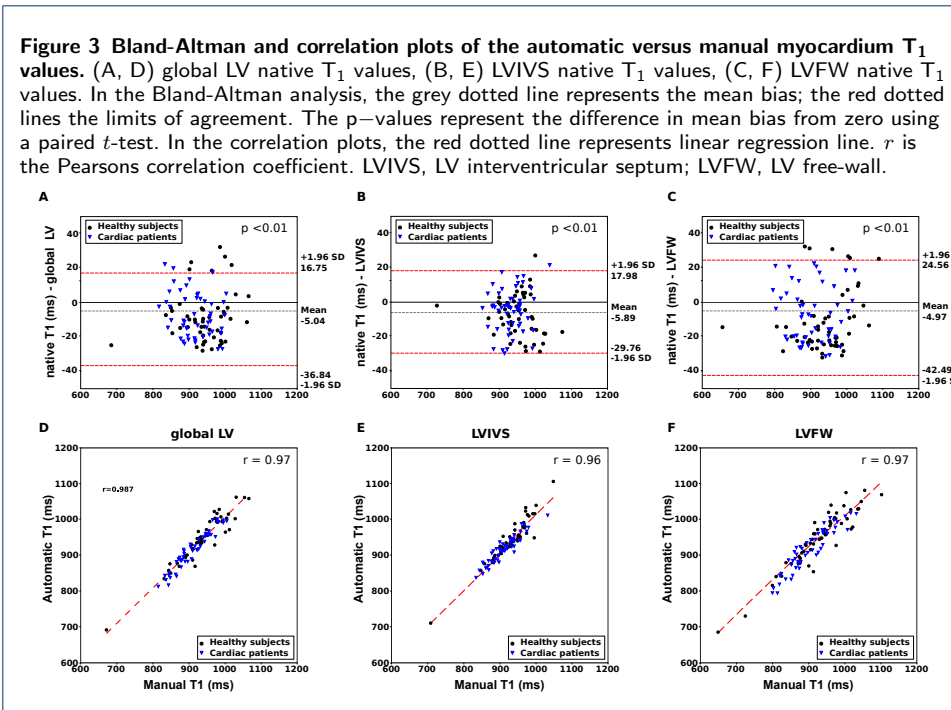
References

1. Baumgartner, C.F., Tezcan, K.C., Chaitanya, K., Hötter, A.M., Muehlematter, U.J., Schawkat, K., Becker, A.S., Donati, O., Konukoglu, E.: PHiSeg: Capturing uncertainty in medical image segmentation. In: Shen, D., Liu, T., Peters, T.M., Staib, L.H., Essert, C., Zhou, S., Yap, P.-T., Khan, A. (eds.) *Medical Image Computing and Computer Assisted Intervention – MICCAI 2019*, pp. 119–127. Springer, Cham (2019)
2. Kim, R.J., Wu, E., Rafael, A., *et al.*: The use of contrast-enhanced magnetic resonance imaging to identify reversible myocardial dysfunction. *New England Journal of Medicine* **343**(20), 1445–1453 (2000)
3. Patel, A.R., Kramer, C.M.: Role of cardiac magnetic resonance in the diagnosis and prognosis of nonischemic cardiomyopathy. *JACC: Cardiovascular Imaging* **10**(10 Part A), 1180–1193 (2017)

4. Sado, D.M., White, S.K., Piechnik, S.K., *et al.*: Identification and assessment of Anderson-Fabry disease by cardiovascular magnetic resonance noncontrast myocardial T1 mapping. *Circulation: Cardiovascular Imaging* **6**(3), 392–398 (2013)
5. Moon, J.C., Messroghli, D.R., Kellman, P., *et al.*: Myocardial T1 mapping and extracellular volume quantification: a society for cardiovascular magnetic resonance (SCMR) and cmr working group of the european society of cardiology consensus statement. *Journal of Cardiovascular Magnetic Resonance* **15**(1), 92 (2013)
6. Nickander, J., Lundin, M., Abdula, G., Sörensson, P., Rosmini, S., Moon, J.C., Kellman, P., Sigfridsson, A., Ugander, M.: Blood correction reduces variability and gender differences in native myocardial T1 values at 1.5T cardiovascular magnetic resonance—a derivation/validation approach. *Journal of Cardiovascular Magnetic Resonance* **19**(1), 41 (2017)
7. Shang, Y., Zhang, X., Zhou, X., Greiser, A., Zhou, Z., Li, D., Wang, J.: Blood T1* correction increases accuracy of extracellular volume measurements using 3T cardiovascular magnetic resonance: Comparison of T1 and T1* maps. *Scientific reports* **8**(1), 3361 (2018)
8. Reiter, U., Reiter, G., Dorr, K., Greiser, A., Maderthaler, R., Fuchsjäger, M.: Normal diastolic and systolic myocardial T1 values at 1.5-T mr imaging: correlations and blood normalization. *Radiology* **271**(2), 365–372 (2013)
9. Bai, W., Sinclair, M., Tarroni, G., *et al.*: Automated cardiovascular magnetic resonance image analysis with fully convolutional networks. *Journal of Cardiovascular Magnetic Resonance* **20**(1), 65 (2018)
10. Ruijsink, B., Puyol-Antón, E., Oksuz, I., Sinclair, M., Bai, W., Schnabel, J.A., Razavi, R., King, A.P.: Fully automated, quality-controlled cardiac analysis from CMR: Validation and large-scale application to characterize cardiac function. *JACC: Cardiovascular Imaging*, 3123 (2019)
11. Fahmy, A.S., El-Rewaify, H., Nezafat, M., Nakamori, S., Nezafat, R.: Automated analysis of cardiovascular magnetic resonance myocardial native T1 mapping images using fully convolutional neural networks. *Journal of Cardiovascular Magnetic Resonance* **21**(1), 7 (2019)
12. Goel, A., McColl, R., King, K.S., Whittmore, A., Peshock, R.M.: Fully automated tool to identify the aorta and compute flow using phase-contrast MRI: Validation and application in a large population based study. *Journal of Magnetic Resonance Imaging* **40**(1), 221–228 (2014)
13. Liu, J.M., Liu, A., Leal, J., McMillan, F., Francis, J., Greiser, A., Rider, O.J., Myerson, S., Neubauer, S., Ferreira, V.M., *et al.*: Measurement of myocardial native T1 in cardiovascular diseases and norm in 1291 subjects. *Journal of Cardiovascular Magnetic Resonance* **19**(1), 74 (2017)
14. Messroghli, D.R., Moon, J.C., Ferreira, V.M., Grosse-Wortmann, L., He, T., Kellman, P., Mascherbauer, J., Nezafat, R., Salerno, M., Schelbert, E.B., *et al.*: Clinical recommendations for cardiovascular magnetic resonance mapping of T1, T2, T2* and extracellular volume: a consensus statement by the society for cardiovascular magnetic resonance (scmr) endorsed by the european association for cardiovascular imaging (eacvi). *Journal of Cardiovascular Magnetic Resonance* **19**(1), 75 (2017)
15. Robinson, R., Valindria, V.V., Bai, W., Oktay, O., Kainz, B., Suzuki, H., Sanghvi, M.M., Aung, N., Paiva, J.M., Zemrak, F., *et al.*: Automated quality control in image segmentation: application to the uk biobank cardiovascular magnetic resonance imaging study. *Journal of Cardiovascular Magnetic Resonance* **21**(1), 18 (2019)
16. Kendall, A., Gal, Y.: What uncertainties do we need in bayesian deep learning for computer vision? In: *Advances in Neural Information Processing Systems*, pp. 5574–5584 (2017)
17. Lakshminarayanan, B., Pritzel, A., Blundell, C.: Simple and scalable predictive uncertainty estimation using deep ensembles. In: *Advances in Neural Information Processing Systems*, pp. 6402–6413 (2017)
18. Zhu, Y., Zabarab, N.: Bayesian deep convolutional encoder–decoder networks for surrogate modeling and uncertainty quantification. *Journal of Computational Physics* **366**, 415–447 (2018)
19. Budd, S., Sinclair, M., Khanal, B., Matthew, J., Lloyd, D., Gomez, A., Toussaint, N., Robinson, E.C., Kainz, B.: Confident head circumference measurement from ultrasound with real-time feedback for sonographers. In: *International Conference on Medical Image Computing and Computer-Assisted Intervention*, pp. 683–691 (2019). Springer
20. Petersen, S.E., Matthews, P.M., Francis, J.M., *et al.*: UK biobanks cardiovascular magnetic resonance protocol. *Journal of cardiovascular magnetic resonance* **18**(1), 8 (2015)
21. Yushkevich, P.A., Piven, J., Hazlett, H.C., Smith, R.G., Ho, S., Gee, J.C., Gerig, G.: User-guided 3D active contour segmentation of anatomical structures: significantly improved efficiency and reliability. *Neuroimage* **31**(3), 1116–1128 (2006)
22. Yang, X.: Understanding the variational lower bound (2017)
23. Simonyan, K., Zisserman, A.: Very deep convolutional networks for large-scale image recognition. *arXiv preprint arXiv:1409.1556* (2014)
24. Seabold, S., Perktold, J.: Statsmodels: Econometric and statistical modeling with python. In: *Proceedings of the 9th Python in Science Conference*, vol. 57, p. 61 (2010). Scipy
25. Lin, K., Suwa, K., Ma, H., Collins, J.D., Markl, M., Carr, J.C.: Variability of native t1 values: implication for defining regional myocardial changes using mri. *The international journal of cardiovascular imaging* **34**(10), 1637–1645 (2018)
26. Ferreira, V.M., Piechnik, S.K., Robson, M.D., Neubauer, S., Karamitsos, T.D.: Myocardial tissue characterization by magnetic resonance imaging: novel applications of t1 and t2 mapping. *Journal of thoracic imaging* **29**(3), 147 (2014)
27. Piechnik, S.K., Ferreira, V.M., Lewandowski, A.J., Ntusi, N.A., Banerjee, R., Holloway, C., Hofman, M.B., Sado, D.M., Maestrini, V., White, S.K., *et al.*: Normal variation of magnetic resonance t1 relaxation times in the human population at 1.5 t using shmoll. *Journal of Cardiovascular Magnetic Resonance* **15**(1), 13 (2013)
28. UK Biobank Register and Apply. <http://www.ukbiobank.ac.uk/register-apply/>. Accessed 20 November 2019

Figures





Tables

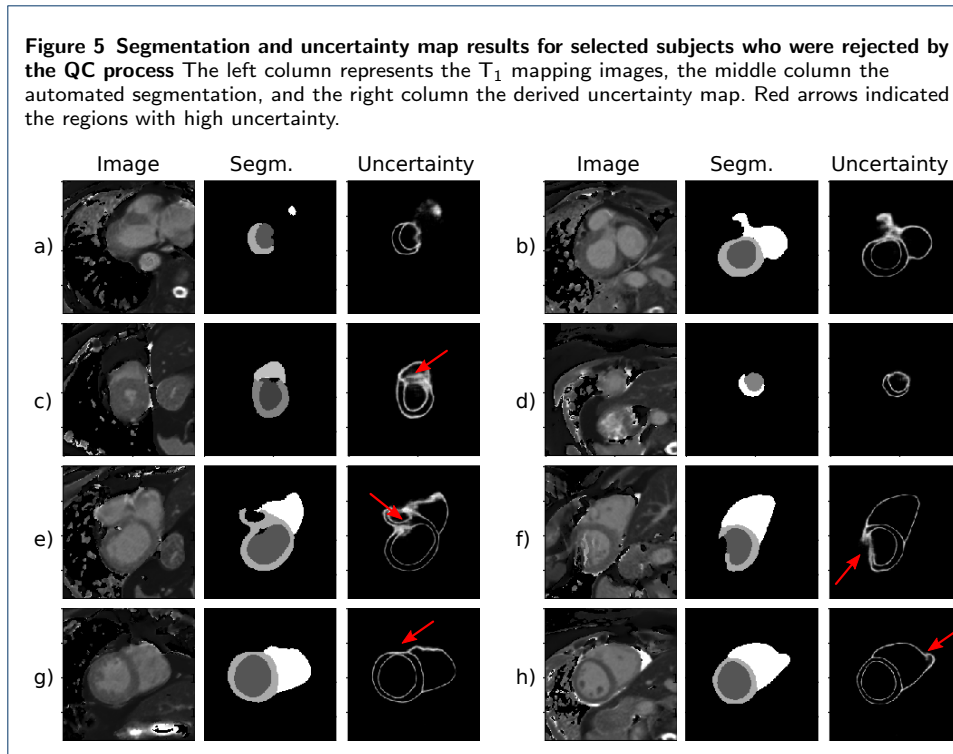


Table 1 Dice score between automated segmentation and manual segmentation for native T₁ images. Dice values are reported as mean (SD).

	Mean dice score		
	LV Blood pool	LV Myocardium	RV blood pool
Healthy (n=50)	0.96 (1.81)	0.83 (3.01)	0.92 (4.23)
Chronic cardiomyopathy (n=50)	0.95 (1.46)	0.84 (3.32)	0.93 (4.06)
Average	0.95 (1.63)	0.84 (3.16)	0.92 (4.14)

Table 2 Mean T₁ values for the test cohort. T₁ are reported as mean (SD). Asterisks indicate significant differences between T₁ values estimated between manual and predicted segmentation using a paired *t*-test.

	Healthy			Chronic cardiomyopathy		
	global LV	LVIVS	LVFW	LV	LVIVS	LVFW
Manual	939.33 (65.51)	947.39 (51.37)	935.65 (76.59)	911.18 (47.90)	930.10 (39.16)	902.04 (57.81)
Automatic	953.99 (66.33)	959.19 (59.08)	952.09 (74.16)	921.40 (51.29)	935.01 (37.36)*	912.72 (59.21)

Table 3 Baseline characteristics of study subjects included in the analysis for reference values. All values are n (%) or mean ± SD. Abbreviations: BMI (body mass index), BSA (body surface area), g (grams), HR (heart rate), kg (kilograms), iLVEDV (indexed LV end-diastolic volume), LVEF (left ventricular ejection fraction), iLVM (indexed LV mass), m (metre). Disease names are as per abbreviations list. * denotes values significantly different from healthy subjects (all *p* < 0.05).

	n	Age (years)	Male (n)	BMI (kg/m ²)	BSA (m ²)	HR (bpm)	iLVEDV(mL/m ²)	LVEF (%)	iLVM (g/m ²)
Healthy	5685	60 (28)	3056 (53.76)	25 (4)	1.84 (0.2)	61 (9)	78 (13)	61 (6)	45 (8)
Acute myocarditis	571	68 (6)	152 (27.19)	28 (5)	1.99 (0.2)	69 (14)	80 (18)	57 (13)	48 (12)
AS	51	68 (7)	15 (29.41)	28 (4)	1.97 (0.2)	73 (5)	83 (23)	59 (6)	56 (13)*
AF	559	68 (6)	152 (27.19)	28 (5)	1.99 (0.2)	72 (11)	80 (18)	51 (9)*	51(11)
Cardiac Sarcoidosis	988	66 (7)	383 (38.77)	30 (6)	2.00 (0.21)	72 (10)	77 (18)	59 (8)	47 (11)
Chronic CAD	1872	67 (7)	576 (30.77)	29 (5)	1.98 (0.2)	60 (10)	79 (18)	48 (9)*	55 (11)*
DCM	567	68 (7)	153 (26.98)	28 (5)	1.99 (0.2)	62 (10)	80 (20)	39 (9)*	56(11)
HCM	571	68 (6)	153 (26.80)	28 (5)	1.99 (0.2)	61 (24)	81 (20)	57 (9)	66 (12)*
Hypertension	973	63 (7)	463 (47.58)	27 (4)	1.91 (0.2)	63 (9)	77 (13)	60 (6)	48 (9)
Phaeochromocytoma	948	66 (7)	364 (38.40)	30 (6)	2.01 (0.21)	62 (10)	78 (18)	58 (9)	46 (15)
Obesity	910	66 (7)	343 (37.69)	30 (6)*	2.12 (0.21)*	62 (10)	78 (19)	59 (8)	45 (11)
Takotsubo cardiomyopathy	988	66 (7)	383 (38.77)	30 (6)	2.01 (0.19)	58 (10)	77 (18)	59 (8)	44 (13)

Additional Files

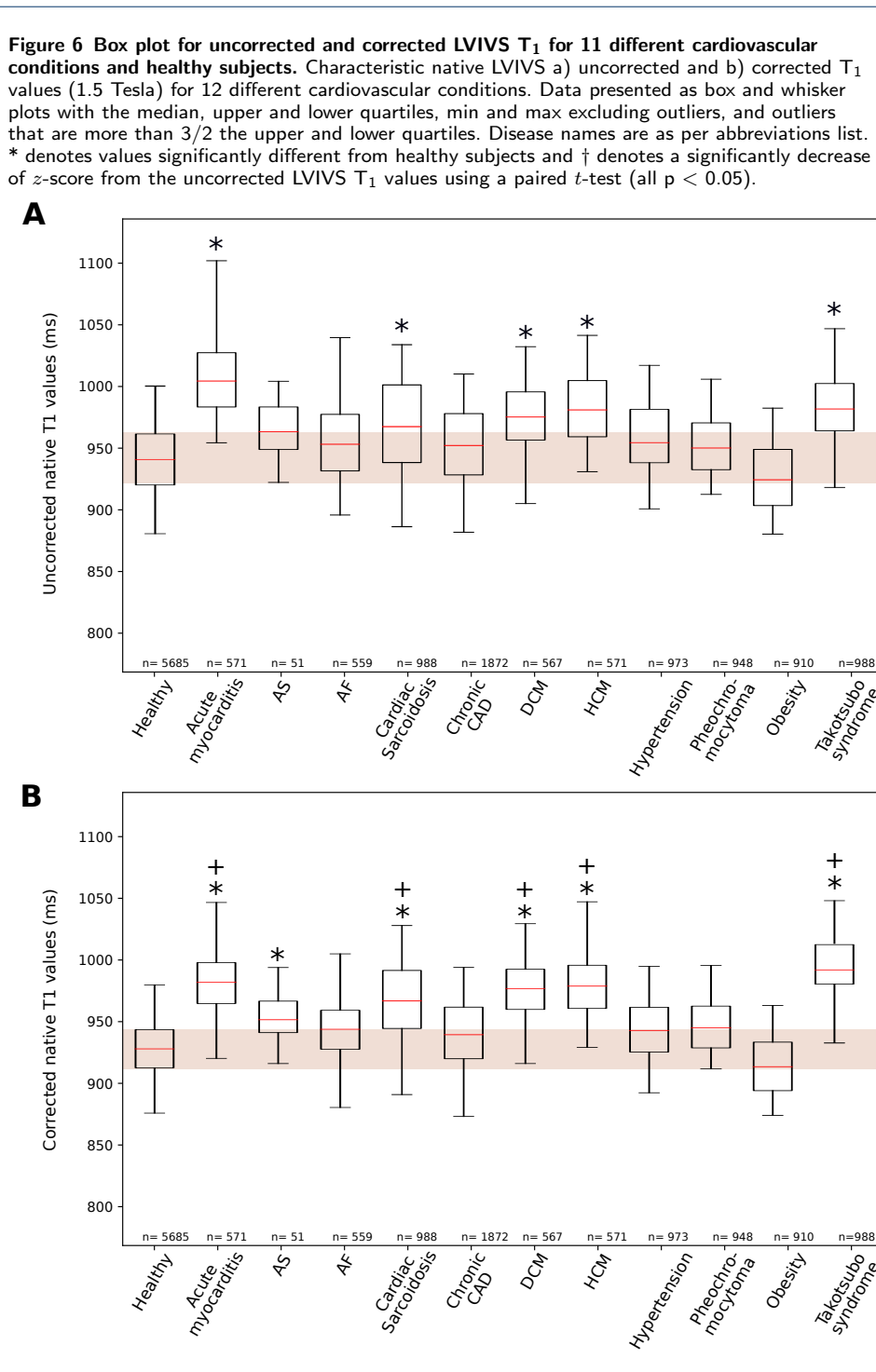


Figure 7 Uncertainty plot for predicted global global LV T₁. Data presented in ascending order of predicted T₁ showing mean T₁ value and SD of uncertainty for each subject. Colours represent the different groups in the test cohort.

Table 4 Age-specific native correlated LVIVS ShMOLLI-T₁ reference ranges. Native T₁ reference ranges detailing mean, lower reference limit and upper reference limit by age group. Reference limits are derived by the upper and lower bounds of the 95% prediction interval for each parameter at each age group. Abbreviation: LVIVS (left ventricle interventricular septum). Disease names are as per abbreviations list.

	45-54			55-64			65-74		
	lower	mean	upper	lower	mean	upper	lower	mean	upper
Healthy	793	930	1066	793	922	1052	781	915	1049
Acute myocarditis	862	973	1084	876	979	1082	853	979	1104
AS		884		851	957	1063	840	956	1072
AF	821	934	1047	838	941	1045	816	941	1066
Cardiac Sarcoidosis	845	950	1055	857	964	1071	838	960	1082
Chronic CAD	822	935	1047	830	940	1050	814	936	1059
DCM	854	965	1076	868	971	1074	846	971	1096
HCM	854	965	1076	868	971	1074	845	971	1096
Hypertension	797	937	1077	814	935	1055	813	941	1068
Pheochromocytoma	822	926	1030	831	937	1044	813	933	1054
Obesity	795	900	1005	807	914	1020	788	909	1030
Takotsubo cardiomyopathy	869	974	1079	881	988	1095	862	984	1106

Table 5 Reference ranges for the native correlated ShMOLLI-T₁ ranges. Reference ranges for the most common myocardial tissue conditions encountered in clinical practice. Abbreviations: LVIVS (left ventricle interventricular septum), LVFW (left ventricle free-wall). Disease names are as per abbreviations list. * denotes values significantly different from healthy subjects (all p < 0.05).

	n	global LV T ₁	T ₁ LVIVS	T ₁ LVFW
Healthy	5685	927.62 (46.41)	922.29 (58.23)	937.34 (40.75)
Acute myocarditis	571	998.39 (50.16)*	972.28 (59.24)*	985.59 (41.23)*
AS	51	954.49 (35.02)	943.42 (40.14)	973.51 (34.08)
AF	559	944.28 (49.71)	935.62 (60.01)	966.34 (40.13)
Cardiac Sarcoidosis	988	972.33 (48.35)*	957.07 (57.40)*	984.18 (40.46)*
Chronic CAD	1872	942.46 (47.18)	933.46 (56.58)	959.25 (38.61)
DCM	567	974.72 (47.18)*	968.71 (59.11)*	990.38 (39.16)*
HCM	571	989.41 (50.16)*	968.68 (55.55)*	989.61 (41.29)*
Hypertension	973	943.75 (49.21)	935.68 (58.24)	958.82 (36.75)
Pheochromocytoma	948	944.23 (48.47)	935.94 (56.68)	963.02 (41.60)
Obesity	910	916.35 (47.73)	907.78 (56.94)	932.45 (41.71)
Takotsubo cardiomyopathy	988	991.82 (48.61)*	983.10 (57.45)*	1009.81 (41.68)*